processes

MDPI

Communication

Neural-Network-Based Nonlinear Model Predictive Control of Multiscale Crystallization Process

Liangyong Wang * and Yaolong Zhu

State Key Laboratory of Integrated Automation for Process Industry, Northeastern University, Shenyang 110819, China
* Correspondence: lywang@mail.neu.edu.cn

Abstract: The purpose of this study was to develop an integrated control strategy for multiscale crystallization processes. An image analysis method using a deep learning neural network is used to measure the fine-scale information of the crystallization process, and the mathematical statistical method is adopted to obtain the mean size of the crystal population. A feedforward neural network is subsequently trained and employed in a nonlinear model predictive control formulation to obtain the optimal profile of the manipulated variable. The effectiveness of the proposed nonlinear model predictive control method is evaluated using alum cooling crystallization experiments. Experimental results demonstrate benefits of the proposed combination of feedforward neural network and nonlinear model predictive control method for the multiscale crystallization process.

Keywords: multiscale crystallization process; image analysis; deep learning; feedforward neural network; nonlinear model predictive control

check for updates

Citation: Wang, L.; Zhu, Y. Neural-Network-Based Nonlinear Model Predictive Control of Multiscale Crystallization Process. *Processes* **2022**, *10*, 2374. https://doi.org/10.3390/pr10112374

Academic Editor: Xiong Luo

Received: 19 September 2022
Accepted: 9 November 2022
Published: 12 November 2022

Publisher's Note: MDPI stays neutral with regard to jurisdictional claims in published maps and institutional affiliations.

1. Introduction

Batch cooling crystallization is widely used in processing industries such as food, medicine, and fine chemicals [1,2]. Multiscale crystallization processes are composed of coupled phenomena covering different length scales [3]. The quality of most crystal products is closely related to microstructural characteristics. In a typical industrial cooling crystallization process, the control of only macro-scale measurable variables (e.g., temperature) is used. A more systematic framework for the modeling and control of multiscale processes is needed [4].

The proposed control methods for crystallization processes in the literature mainly include model-based control, model-free control, and machine-learning-based control [5]. Multiscale crystallization processes can be represented through partial differential equation(PDE)/ordinary differential equation (ODE)kinetic Monte Carlo (kMC) approximations [6,7]. The multiscale model of the crystallization process cannot be employed in the controller design due to the distributed nature of PDEs and the non-closed form of kMC. Hence, the order of the model needs to be reduced, which can capture the dominant dynamic and reduce computational cost [8,9]. Díez et al. [10] interpreted discretized population balance models (PBMs) as chemical reaction networks and designed an inventory controller. Ghadipasha et al. [11] proposed several model-based control methods, including linearizing feedback control, internal model control, and output feedback control. Szilágyi et al. [12] designed a nonlinear model predictive control (NMPC) method which operates by estimating crystal nucleation and growth kinetic parameters from measurements of solution concentration and chord length distribution (CLD). However, model-based order-reduced methods are dependent on the mechanism model of the crystallization process. If this mechanism model is poorly designed, model mismatch can degrade the control performance. Model-free control schemes such as supersaturation control (SSC) and direct nucleation control (DNC) can be used to indirectly control final crystal properties

by manipulating super-saturation or the number of crystals measured in real time. It is more difficult to evaluate the optimality of the operation using model-free control schemes due to their heuristic nature. Recently, machine-learning-based control methods have been applied to multiscale processes [13–17]. Griffin et al. [13] proposed a data-driven modeling method using machine learning and a control method based on dynamic programming. Manee et al. [14] presented a reinforcement learning (RL) controller to drive the target mean size and the target standard deviation. Model predictive control (MPC)can deal with multi-variable interactions, input and state constraints as well as optimization requirements. The use of machine learning in MPC formulations has proven to be a promising approach for multiscale processes [15–17]. Kimaev et al. [16] proposed an artificial-neural-network-based NMPC method for a multiscale thin-film deposition process. However, the proposed methods present only simulation results and have not been applied in multiscale crystallization processes.

The measurement of the fine-scale information of crystallization processes is a challenging task [4]. At present, common measurement tools mainly include Coulter counter [18], laser diffraction [18], focused beam reflection measurement (FBRM) [19], and image processing algorithms [20]. The measurement accuracy of the Coulter counter, laser diffraction, and FBRM methods is not ideal. In general, a crystal particle can be observed by optical microscope if the crystal size exceeds 0.5 μm [6]. Traditional image processing algorithms suffer from problems such as processing speed and human intervention. At present, deep-learning-based crystal image analysis methods have been developed, representing end-to-end tools requiring no human intervention once the deep learning network has been trained. Moreover, instance segmentation methods based on deep learning can complete segmentation tasks in a pixel-to-pixel manner [21–23], which provides a promising tool for the measurement of the fine-scale information of crystallization processes.

The main goal of this paper is to provide an integrated control strategy for multiscale batch cooling crystallization processes. An image analysis method using a deep learning neural network is used to measure the fine-scale information of the crystallization process and a mathematical statistical method is adopted to obtain the mean size of the crystal population. Based on the available measurement of microstructural characteristics, the resulting NMPC method is developed from the neural network model. On this basis, the NMPC model is designed and implemented. Alum cooling crystallization experiments were carried out to verify the feasibility and effectiveness of the proposed control strategy.

2. Multiscale Dynamical Model Description

A multiscale model for describing the dynamic evolution of a crystallization process is introduced in the following.

2.1. Macroscopic Model

The macroscopic mass and energy balance equations [24] are expressed as:

$$\frac{\mathrm{d}C}{\mathrm{d}t} = -3\rho k_{\mathrm{v}} G(t) \int_0^{r_{\max}} r^2 \gamma(r,t)\mathrm{d}r, \tag{1}$$

$$\frac{\mathrm{d}T}{\mathrm{d}t} = -\frac{UA}{MC_{\mathrm{p}}}(T - T_{\mathrm{j}}) - \frac{\Delta H}{C_{\mathrm{p}}} 3\rho k_{\mathrm{v}} G(t) \int_0^{r_{\max}} r^2 \gamma(r,t)\mathrm{d}r, \tag{2}$$

where $\gamma(r,t)$ is the number density function, r is the characteristic crystal size, C is the solute concentration, T is the solution temperature, and $G(t)$ is the crystal growth rate. ρ is the density of crystal, $r_{\max}$ is the maximum particle radius, k_{v} is the volumetric shape factor, U is the overall heat-transfer coefficient, A is the total heat-transfer surface area, M is the mass of solvent in the crystallizer, C_{p} is the heat capacity of the solution, T_{j} is the jacket temperature, and ΔH is the heat of reaction.

2.2. Mesoscopic Model

In this paper, a seeded crystallization process is considered. Moreover, the proposed control method is applied to the growth-dominant crystallization stage, and the nucleation process is not considered in this paper. Assuming that the solution in the crystallizer is evenly mixed, the evolution of the number density function under the influence of growth is governed by the PBM [24]:

$$\frac{\partial \gamma(r,t)}{\partial t} + \frac{G(t)\partial \gamma(r,t)}{\partial r} = 0. \tag{3}$$

2.3. Microscopic Model

The solid-on-solid model [3], which was developed to model crystal growth processes accounting for surface microstructure, is employed to model the growth of crystals as follows. The solid-on-solid model is composed of an adsorption rate model, desorption rate model, and migration rate model.

The adsorption rate is defined as

$$r_{\mathrm{a}} = K_0^+ \exp\left(\frac{\Delta\mu}{k_{\mathrm{B}}T}\right), \tag{4}$$

where K_0^+ is the attachment coefficient, k_{B} is the Boltzmann constant, and Äì = $k_{\mathrm{B}}T \ln(C/S)$, where S is solubility and Äì is the crystal growth driving force.

The desorption rate is given by

$$r_{\mathrm{d}}(i) = K_0^- \exp\left(-i\frac{E_{\mathrm{pb}}}{k_{\mathrm{B}}T}\right), \tag{5}$$

where K_0^- is the desorption coefficient, i is the number of bonds, and E_{pb} is the average binding energy per bond.

The migration rate, which describes the migration to the interfacial molecule to stronger binding sites, is defined as

$$r_{\mathrm{m}}(i) = K_0^+ \exp\left(\frac{\phi}{k_{\mathrm{B}}T} - i\frac{E_{\mathrm{pb}}}{k_{\mathrm{B}}T} + \frac{E_{\mathrm{pb}}}{2k_{\mathrm{B}}T}\right). \tag{6}$$

The growth rate cannot be computed by simply subtracting the adsorption rate, the desorption rate, and the migration rates, and requires the use of kMC simulations. Each event in the kMC simulation is chosen randomly on the basis of the adsorption rate, the desorption rate, and the migration rate.

As mentioned above, the crystallization process can be described by macroscale model, mesoscale model, and microscale model. Hence, the multiscale model of the crystallization process is summarized in Figure 1, where the information transfer among the different scales is demonstrated by black directional arrows. However, the multiscale model expressed by PDE/ODEs kMC cannot be incorporated in the model-based optimization and control due to the distributed nature of PDE and the non-closed form of kMC. Additionally, since the objective of the crystallization process is to obtain desired crystal characteristics (i.e., mean size $\overline{\gamma}$), the NMPC is formulated to manipulate input (i.e., temperature T_{j}) to achieve a desired mean size. In order to deal with these problems, neural network approaches can be utilized for the crystallization processes.

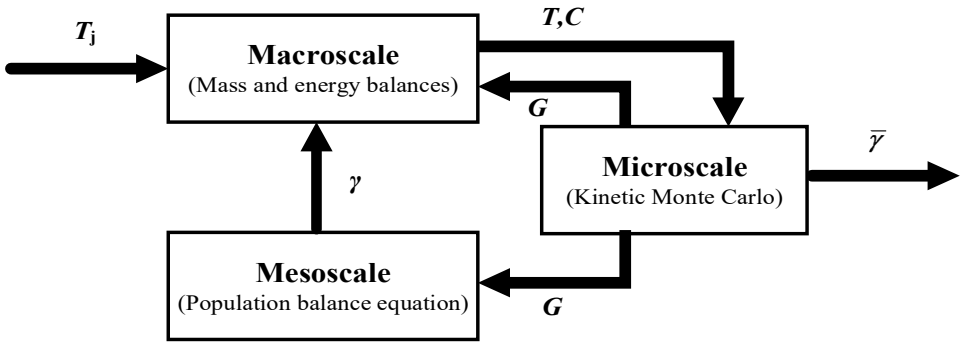

Figure 1. Multiscale scheme of the crystallization model.

3. Model and Controller Design of NMPC

For the control of the multiscale crystallization process, NMPC is a natural choice that can explicitly cope with nonlinearities and constraints while minimizing a performance objective. In this section, a deep-learning-based method for the on-line measurement of microscale characteristic is presented. Then, the design of a feedforward neural network model of multiscale crystallization processes is described. Finally, we describe the development of an NMPC scheme for the multiscale crystallization process.

3.1. Deep-Learning-Based On-Line Measurement Method

As mentioned above, the modeling and control of multiscale crystallization processes requires knowledge of the microscale characteristics of the crystallization process. To this end, the real-time detection of crystal particles and information extraction of the crystal size are realized using a Mask Regional Convolutional Neural Network (Mask R-CNN). A Mask R-CNN can perform various tasks, such as object detection, classification, semantic segmentation, and instance segmentation [25]. Instance segmentation methods based on deep learning can complete segmentation tasks in a pixel-to-pixel manner, which provides a promising measurement tool for the fine-scale information of crystallization processes. The mask branch of the Mask R-CNN produces a binary image, where the crystals are separated from the background of the binary image. Moreover, a pixel-level map is obtained through the crystal objects represented by different colors, and the relevant parameters of the crystal can be extracted and calculated using the pixel-level map. Hence, crystals can be described in terms of their area, the length of the axis of the fitting ellipse, and area-equivalent diameter, which can be extracted and calculated using the pixel-level map. Finally, the crystal mean size can be obtained through mathematical statistical analysis [26–28]. The flowchart of the real-time analysis of crystal images based on Mask R-CNN is shown in Figure 2. An original image and its output results from the Mask R-CNN are presented in Figures 3 and 4, respectively. A detailed description of the instance segmentation method based on deep learning can be seen in Gan et al. (2022) [29].

3.2. Feedforward Neural Network Model

As can be seen in Figure 1, the crystal mean size $\overline{\gamma}$ and the jacket temperature T_j can be defined as the output y and manipulated input u, respectively. The input-to-output dynamics of multiscale crystallization process can be presented as:

$$y(k+1) = f\left[y(k), \ldots, y(k-n_y), u(k), \ldots, u(k-n_u)\right], \tag{7}$$

where n_y and n_u represent the number of lagged outputs and inputs required for prediction, respectively.

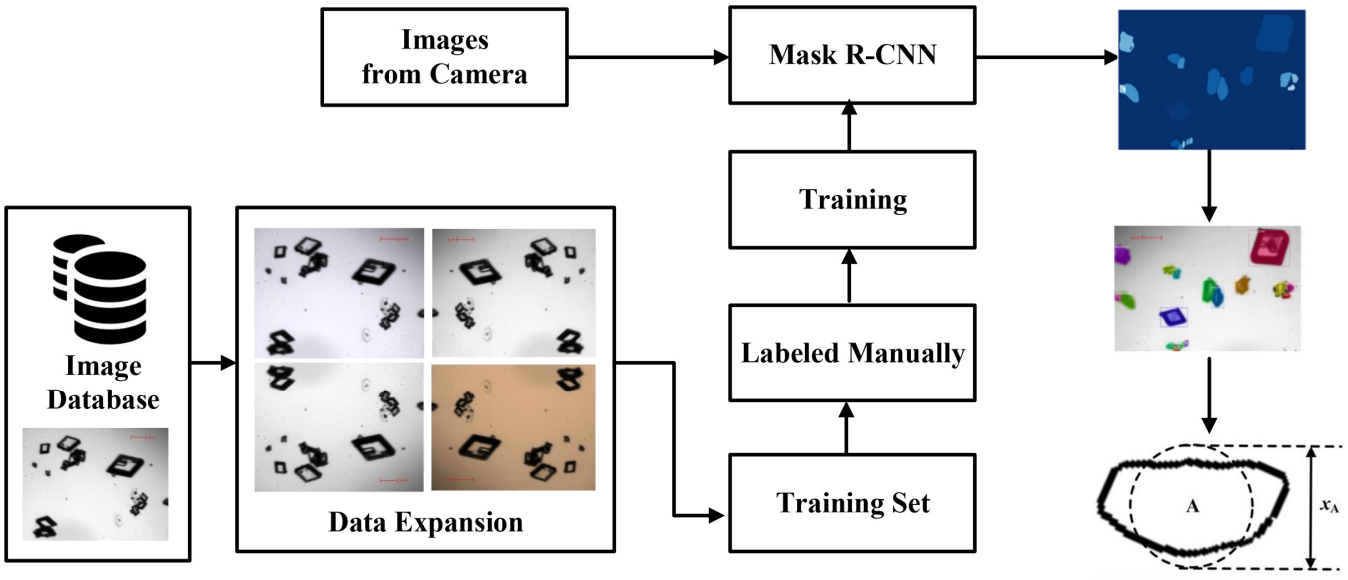

Figure 2. Real-time crystal image analysis process based on Mask R-CNN.

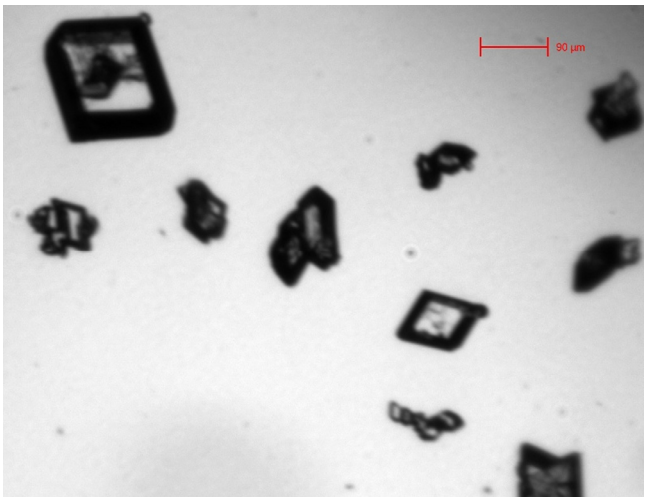

Figure 3. Original crystal image.

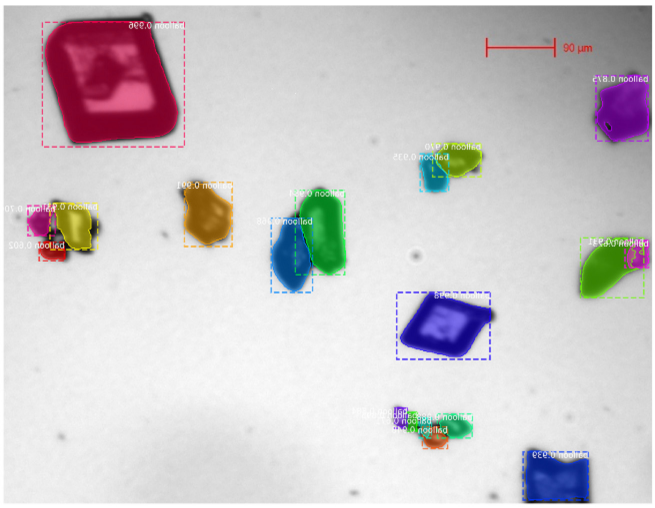

Figure 4. Output results of Mask R-CNN.

In this paper, a feedforward neural network (FNN) [30] is used to model the dynamic behavior of the system. The neural network model can be represented by

$$y_{\mathrm{m}}(k+1) = f_{\mathrm{NN}}\left[y(k), \ldots, y(k-n_y), u(k), \ldots, u(k-n_u)\right], \tag{8}$$

where $y_{\mathrm{m}}(k+1)$ is the output of the neural network.

Given the complex dynamics within the crystallization process, a well-designed FNN would be able to capture the dominant dynamics of the multiscale crystallization process. To approximate the nonlinear mapping function $f(\bullet)$, a class of feedforward neural networks can be used. A schematic of the developed FNN is shown in Figure 5. In this paper, the hyperbolic tangent sigmoid transfer function is used for the neurons in the hidden layer(s), and a linear transfer function is utilized for the neurons in the output layer. The output of the hidden nodes is

$$N_j = f_h\left(\sum_{i=1}^{n} W_{ij}x_i + B_j\right), \tag{9}$$

where N denotes the neuron, W denotes the weight matrix, and B denotes the bias matrix. In each equation, i and j refer to the index of neurons in the previous and the subsequent layer. n describes the number of neurons in the input layer. The hyperbolic tangent sigmoid function is expressed as:

$$f_h(x) = \frac{2}{1+\exp(-2x)} - 1. \tag{10}$$

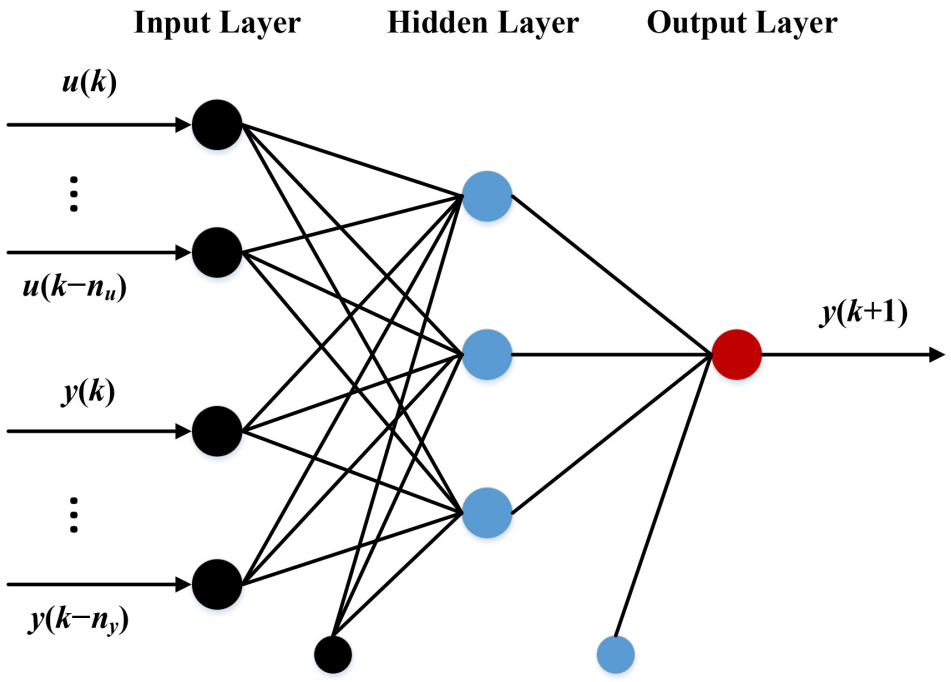

Figure 5. Schematic diagram of the developed FNN.

3.3. Nonlinear Model Predictive Controller Design

In this paper, the above FNN is employed to develop the nonlinear model predictive control of a multiscale crystallization process. The neural network model predicts the response over a specified time horizon. The model predictive control method is expressed as

$$\begin{aligned} \min J = & \sum_{i=0}^{p-1} \|y_{\mathrm{d}}(k+i) - y_{\mathrm{m}}(k+i)\|^2 + a \sum_{i=0}^{m-1} \{u(k+i) - u(k+i-1)\}^2 \\ \text{s.t. } & y_{\mathrm{m}}(k+1) = f_{\mathrm{NN}}\left[y(k), \ldots, y(k-n_y), u(k), \ldots, u(k-n_u)\right] \\ & u_{\min} \leq u(k) \leq u_{\max} \\ & \Delta u_{\min} \leq \Delta u(k) \leq \Delta u_{\max} \end{aligned} , \quad (11)$$

where $y_{\mathrm{d}}(k+i)$ is the target mean size. p and m define the prediction horizon and control horizon, respectively. a determines the contribution of the control increment to the performance index. $u_{\min}$ and $u_{\max}$ are the constraints on the manipulated variable. $\Delta u(k) = u(k) - u(k-1)$. $\Delta u_{\min}$ and $\Delta u_{\max}$ are the minimum and maximum gradients of the manipulated variable, respectively.

4. Material and Methods

The experimental equipment for the batch cooling crystallization processes is shown in Figure 6. The experimental equipment is composed of a batch crystallizer, invasive camera probe, variable-speed paddle stirrer, heating and cooling system, and industrial computers. The setpoint of the temperature controller is provided by the higher-level NMPC. The NMPC algorithm is implemented in an industrial computer. In this paper, high-purity alum ($KAl(SO_4)_2 \cdot 12H_2O$) is selected as the crystallization material. In the experimental stage, 1500 g of distilled water and 165 g of high-purity alum produced by Aladdin are added into the crystallizer. The stirring speed is set to 130 r/min to make the solution evenly mixed. The experimental process is as follows. First, the temperature of the solution is rapidly raised to 35 °C by a thermostatic controller and kept at 35 min until the high-purity alum is completely dissolved. Then, the temperature is rapidly reduced to 20 °C, maintained for 10 min, and then reduced to 19 °C at a rate of 0.1 °C/min. At this point, the solution is at a supersaturated state. Then, 7 g of the seed crystals are put into the crystallizer. Once it is observed from the invasive camera that the crystallization process enters the growth-dominant crystallization stage, the proposed control methods are put into use. The target size is set at 470 μm.

Figure 6. Experimental equipment for batch cooling crystallization processes.

The neural network training process is implemented using the Neural Net Time Series toolbox in MATLAB. The Levenberg–Marquardt backpropagation method is used for tuning the weights and biases. Furthermore, the FNN architecture is trained and tested with 4 inputs, one hidden layer with 10 neurons, and 1 output. Specifically, Figure 7

shows that the predicted crystal mean size from the FNN and the experimental data are in excellent agreement. To evaluate the fit performance, the following index is defined as $\left[1-\sqrt{\sum_{i=1}^{n}(y(i)-y_{\mathrm{m}}(i))^2}\Big/\sqrt{\sum_{i=1}^{n}(y(i)-\overline{y})^2}\right]*100\%$, where y is the measured output, y_{m} is the predicted model output, and $\overline{y}$ is the mean value of y. The fit index is computed as 98.2%. In this study, the experimental data of 20 batch runs are collected. The experimental data sets are used for training (60%), validation (10%), and testing (30%). If the experimental data sets were further expanded, the fit performance of the FNN could be enhanced.

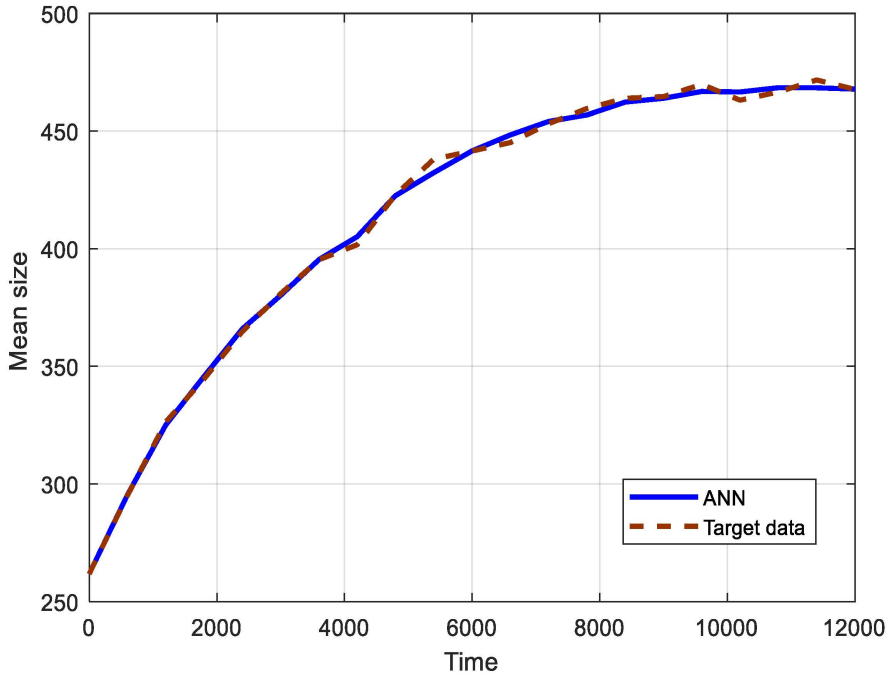

Figure 7. Validation of the ANN compared to the target experimental data.

5. Experimental Results

In the above section, the NMPC scheme is developed for a multiscale crystallization process. The experimental results of the NMPC method are shown in Figures 8 and 9. Figure 8 shows the trajectories of mean crystal size. The mean size generally follows the target values. Figure 9 shows the trajectory of the control input by the NMPC. It can be seen from Figure 9 that NMPC controls the temperature in the crystallizer through heating or cooling in order to make the crystal mean size track the target values. Proportional integral derivative (PID) is a model-free control method requiring no crystal model. The experimental material and conditions are the same as that of the NMPC. The experimental results of PID are shown in Figures 10 and 11. Figure 10 presents the trajectories of mean crystal size. Figure 11 demonstrates the trajectory of control input for the PID method.

The control performance can be evaluated by the maximum error and the integral square error. The maximum errors of NMPC and PID at steady state are 5.3 μm and 9.2 μm, respectively. The integral square errors of NMPC and PID at steady state are 162.5 and 333.2, respectively. It can be concluded that the developed NMPC method was tested and proven to perform well with significant improvements over PID controllers due to the prediction and optimization capabilities of the NMPC. Although mean crystal size is a key feature of crystal size distribution, a method for the control of the overall crystal size distribution is still required to further improve the quality of the crystal product.

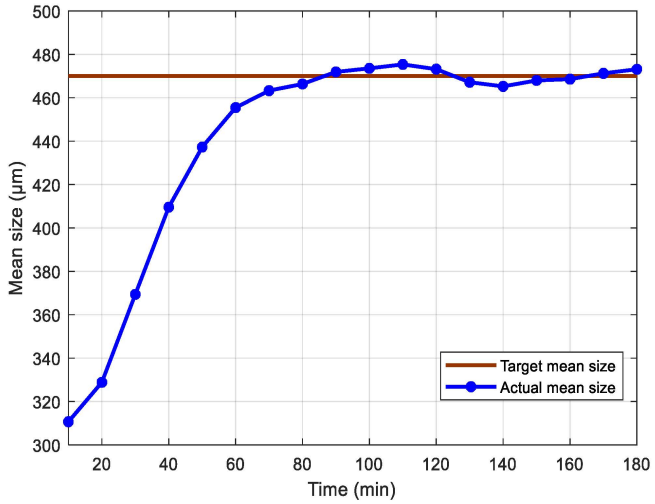

Figure 8. Mean crystal size profiles for NMPC.

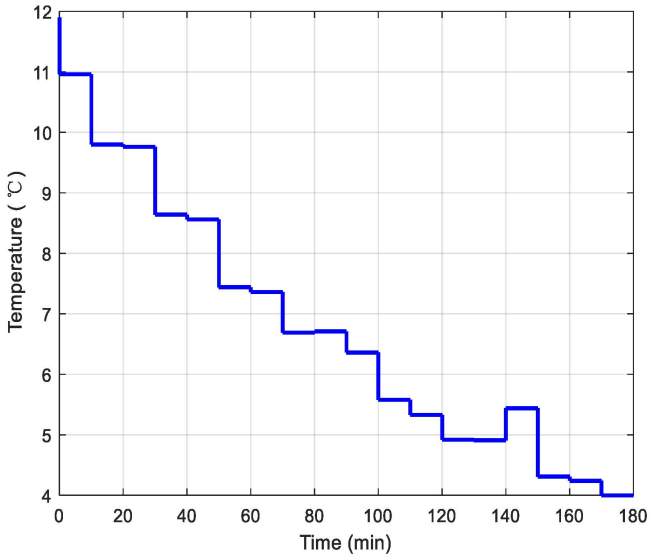

Figure 9. Control input profile for NMPC.

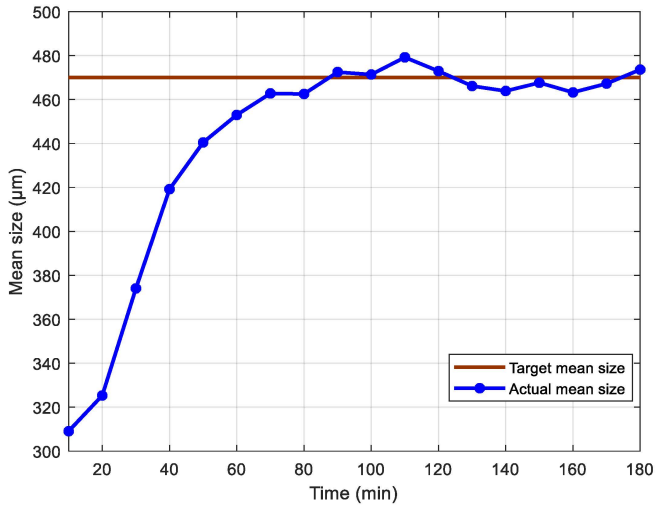

Figure 10. Mean crystal size profiles for PID.

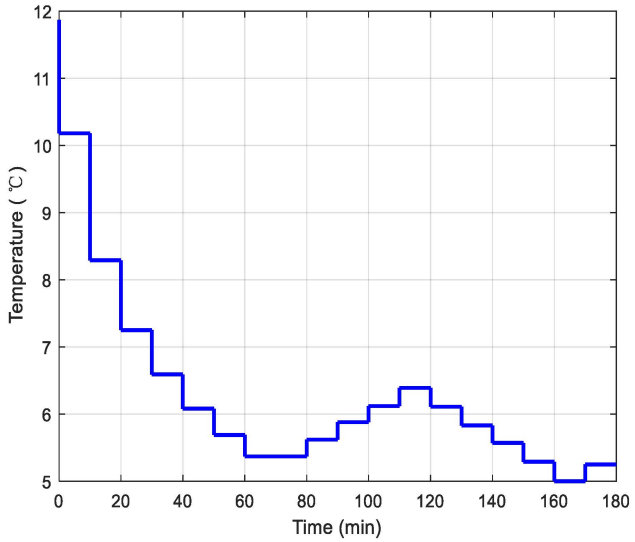

Figure 11. Control input profile for PID.

6. Conclusions

This paper proposes an NMPC method which takes the mean crystal size as the manipulated variable. A deep-learning-based image analysis method and mathematical statistical technique were developed to measure the mean size. Based on the available measurements, the resulting nonlinear prediction model for the NMPC was developed using a neural network. Alum cooling crystallization experiments were carried out to verify the feasibility and effectiveness of the proposed NMPC strategy. The paper demonstrates a solid example of the design and control of a multiscale process.

Author Contributions: Conceptualization, L.W.; methodology, L.W.; software, Y.Z.; validation, Y.Z.; formal analysis, L.W.; investigation, L.W.; writing—original draft preparation, L.W.; writing—review and editing, L.W.; project administration, L.W.; funding acquisition, L.W. All authors have read and agreed to the published version of the manuscript.

Funding: This research was funded by Shenyang young and middle-aged scientific and technological innovation talents program under Grant No.RC200519.

Institutional Review Board Statement: Not applicable.

Informed Consent Statement: Not applicable.

Data Availability Statement: Not applicable.

Conflicts of Interest: The authors declare no conflict of interest. The funders had no role in the design of the study; in the collection, analysis, or interpretation of the data; in the writing of the manuscript; or in the decision to publish the results.

References

1. Rawlings, J.B.; Miller, S.M.; Witkowski, W.R. Model Identification and Control of Solution Crystallization Processes: A Review. *Ind. Eng. Chem. Res.* **1993**, *32*, 1275–1296. [CrossRef]
2. Braatz, R.D. Advanced control of crystallization processes. *Annu. Rev. Control* **2002**, *26*, 87–99. [CrossRef]
3. Kwon, J.S.-I.; Nayhouse, M.; Christofides, P.D. Multiscale, multidomain modeling and parallel computation: Application to crystal shape evolution in crystallization. *Ind. Eng. Chem. Res.* **2015**, *54*, 11903–11914. [CrossRef]
4. Ricardez-Sandoval, L.A. Current challenges in the design and control of multiscale systems. *Can. J. Chem. Eng.* **2011**, *89*, 1324–1341. [CrossRef]
5. Montes, F.C.C.; Öner, M.; Gernaey, K.V.; Sin, G. Model-Based Evaluation of a Data-Driven Control Strategy: Application to Ibuprofen Crystallization. *Processes* **2021**, *9*, 653. [CrossRef]
6. Kwon, J.S.-I.; Nayhouse, M.; Christofides, P.D.; Orkoulas, G. Modeling and control of protein crystal shape and size in batch crystallization. *AIChE J.* **2013**, *59*, 2317–2327. [CrossRef]

7. Urrea-Quintero, J.-H.; Ochoa, S.; Hernández, H. A reduced-order multiscale model of a free-radical semibatch emulsion polymerization process. *Comput. Chem. Eng.* **2019**, *127*, 11–24. [CrossRef]
8. Chiu, T.; Christofides, P. Nonlinear control of particulate processes. *AIChE J.* **1999**, *45*, 1279–1297. [CrossRef]
9. Chiu, T.; Christofides, P. Robust control of particulate processes using uncertain population balances. *AIChE J.* **2000**, *46*, 266–280. [CrossRef]
10. Díez, M.D.; Ydstie, B.E.; Fjeld, M.; Lie, B. Inventory control of particulate processes. *Comput. Chem. Eng.* **2008**, *32*, 46–67. [CrossRef]
11. Ghadipasha, N.; Romagnoli, J.A.; Tronci, S.; Baratti, R. A Model-Based Approach for Controlling Particle Size Distribution in Combined Cooling-Antisolvent Crystallization Processes. *Chem. Eng. Sci.* **2018**, *190*, 260–272. [CrossRef]
12. Szilágyi, B.; Agachi, P.S.; Nagy, Z.K. Chord Length Distribution Based Modeling and Adaptive Model Predictive Control of Batch Crystallization Processes Using High Fidelity Full Population Balance Models. *Ind. Eng. Chem. Res.* **2018**, *57*, 3320–3332. [CrossRef]
13. Griffin, D.J.; Grover, M.A.; Kawajiri, Y.; Rousseau, R.W. Data-Driven Modeling and Dynamic Programming Applied to Batch Cooling Crystallization. *Ind. Eng. Chem. Res.* **2016**, *55*, 1361–1372. [CrossRef]
14. Manee, V.; Baratti, R.; Romagnoli, J.A. Learning to navigate a crystallization model with deep reinforcement learning. *Chem. Eng. Res. Des.* **2022**, *178*, 111–123. [CrossRef]
15. Chaffart, D.; Ricardez-Sandoval, L.A. Optimization and control of a thin film growth process: A hybrid first principles/artificial neural network based multiscale modelling approach. *Comput. Chem. Eng.* **2018**, *119*, 465–479. [CrossRef]
16. Kimaev, G.; Ricardez-Sandoval, L.A. Nonlinear model predictive control of a multiscale thin film deposition process using Artificial Neural Networks. *Chem. Eng. Sci.* **2019**, *207*, 1230–1245. [CrossRef]
17. Sitapurea, N.; Kwon, J.S.-I. Neural network-based model predictive control for thin-film chemical deposition of quantum dots using data from a multiscale simulation. *Chem. Eng. Res. Des.* **2022**, *183*, 595–607. [CrossRef]
18. Nagy, Z.K.; Braatz, R.D. Advances and New Directions in Crystallization Control. *Annu. Rev. Chem. Biomol. Eng.* **2012**, *3*, 55–75.
19. Ruf, A.; Worlitschek, J.; Mazzotti, M. Modeling and Experimental Analysis of PSD Measurements through FBRM. *Part. Part. Syst. Charact.* **2000**, *17*, 167–179. [CrossRef]
20. Zhang, B.; Willis, R.; Romagnoli, J.A.; Fois, C.; Tronci, S.; Baratti, R. Image-Based Multi-resolution ANN Approach for Online Particle Size Characterization. *Ind. Eng. Chem. Res.* **2014**, *53*, 7008–7018. [CrossRef]
21. Gao, Z.; Wu, Y.; Bao, Y.; Gong, J.; Wang, J.; Rohani, S. Image Analysis for In-line Measurement of Multidimensional Size, Shape, and Polymorphic Transformation of L-Glutamic Acid Using Deep Learning-Based Image Segmentation and Classification. *Cryst. Growth Des.* **2018**, *18*, 4275–4281. [CrossRef]
22. Wang, L.; Zhu, Y.; Gan, C. Predictive control of particle size distribution of crystallization process using deep learning based image analysis. *AIChE J.* 2022, *in press*.
23. Manee, V.; Zhu, W.; Romagnoli, J.A. A Deep Learning Image-Based Sensor for Real-Time Crystal Size Distribution Characterization. *Ind. Eng. Chem. Res.* **2019**, *58*, 23175–23186. [CrossRef]
24. Shi, D.; El-Farra, N.; Li, M.; Mhaskar, P.; Christofides, P. Predictive control of particle size distribution in particulate processes. *Chem. Eng. Sci.* **2006**, *66*, 268–281. [CrossRef]
25. He, K.; Gkioxari, G.; Dollár, P.; Girshick, R. Mask R-CNN. In Proceedings of the IEEE International Conference on Computer Vision, Venice, Italy, 22–29 October 2017; pp. 2980–2988.
26. Zhang, L.C.; Xu, W.Y.; Li, Z.; Zheng, L.; Liu, Y.F.; Zhang, G.Q. Characterization of particle shape of nickel-based superalloy powders using image processing techniques. *Powder Technol.* **2022**, *395*, 787–801. [CrossRef]
27. Faria, N.; Pons, M.N.; De Azevedo, S.F.; Rocha, F.A.; Vivier, H. Quantification of the morphology of sucrose crystals by image analysis. *Powder Technol.* **2003**, *133*, 54–67. [CrossRef]
28. Souza, D.; Menegalli, F.C. Image analysis: Statistical study of particle size distribution and shape characterization. *Powder Technol.* **2011**, *21*, 57–63. [CrossRef]
29. Gan, C.; Wang, L.; Zhu, Y. Feedback Control of Crystal Size Distribution for Cooling Batch Crystallization Using Deep Learning-Based Image Analysis. *Crystals* **2022**, *12*, 570. [CrossRef]
30. Atuonwu, J.C.; Cao, Y.; Rangaiah, G.P.; Tadé, M.O. Identification and predictive control of a multistage evaporator. *Control Eng. Pract.* **2010**, *18*, 1418–1428.